Single-Shot Readout of a Solid-State Electron Spin Qutrit

Yuhang Guo,[1,2] Wentao Ji,[1,2,4] Xi Kong,[3,*] Mengqi Wang,[1,2,4] Haoyu Sun,[1,2] Jingyang Zhou,[1,2] Zihua Chai,[1,2] Xing Rong,[1,2,4] Fazhan Shi,[1,2,4] Ya Wang,[1,2,4,†] and Jiangfeng Du[1,2,4,5,‡]

[1]*CAS Key Laboratory of Microscale Magnetic Resonance and School of Physical Sciences, University of Science and Technology of China, Hefei 230026, China*

[2]*CAS Center for Excellence in Quantum Information and Quantum Physics, University of Science and Technology of China, Hefei 230026, China*

[3]*The State Key Laboratory of Solid State Microstructures and Department of Physics, Nanjing University, Nanjing 210093, China*

[4]*Hefei National Laboratory, University of Science and Technology of China, Hefei 230088, China*

[5]*School of Physics, Zhejiang University, Hangzhou 310027, China*

(Received 6 July 2023; accepted 9 January 2024; published 8 February 2024)

Quantum systems usually feature a rich multilevel structure with promising resources for developing superior quantum technologies compared with their binary counterpart. Single-shot readout of these high-dimensional quantum systems is essential for exploiting their potential. Although there have been various high-spin systems, the single-shot readout of the overall state of high-spin systems remains a challenging issue. Here we demonstrate a reliable single-shot readout of spin qutrit state in a low-temperature solid-state system utilizing a binary readout scheme. We achieve a single-shot readout of an electron spin qutrit associated with a single nitrogen-vacancy center in diamond with an average fidelity of 87.80%. We use this spin qutrit system to verify quantum contextuality, a fundamental test of quantum mechanics. We observe a violation of the noncontextual hidden variable inequality with the developed single-shot readout in contrast to the conventional binary readout. These results pave the way for developing quantum information processing based on spin qutrits.

DOI: 10.1103/PhysRevLett.132.060601

After decades of development, quantum information science has become one of the most important research fields. While most current research focuses on qubits, qudit-based systems have gained substantial interest due to significant advantages. Qudits exhibit distinguished properties in quantum communication compared to qubits, including larger channel capacity, better noise resistance, and higher security [1–4]. In quantum computation, qudits can also provide obvious advantages, including smaller code size [5], robust cryptography protocols [6], and more efficient quantum circuits [7–9]. Moreover, qudits show stronger violations of Bell inequality [10,11] and make the testing of contextuality feasible [12–15] compared to qubits in fundamental tests of quantum mechanics.

Qutrit, the simplest form of qudit, has been experimentally explored in various systems, such as superconducting transmon circuits [16,17], photonic systems [4,12], trapped ions [18], and spin-1 systems. Among spin-1 systems, nitrogen-vacancy (NV) centers in diamond have become a versatile platform thanks to superior properties, such as long coherence time, spin-optical interface, and on-demand unitary operation. NV centers have been utilized for quantum sensing [19–22], quantum communication [23–26], quantum information processing [27,28], and fundamental tests of quantum mechanics [29–31]. However, while most research utilizes NV centers as qubits, only a few studies can actually exploit the potential of NV centers as qutrits [32,33]. One main obstacle is the lack of the single-shot readout of electron spin qutrit. The main difficulties lie in the incompatibility between the destructive measurement and binary readout schemes. A nondemolition binary measurement is necessary to avoid the destruction of the qutrit state after the first binary readout [Fig. 1(a)]. However, due to spin-flip errors in the excited state [34] and poor photon collection efficiency, the electron spin state is destroyed after measurement. To address this challenge, we demonstrate a new path to realize a single-shot readout of NV center electron spin qutrit in diamond merely at the expense of multicolor excitation.

The basic idea of our scheme is mapping one fragile spin state to a state that is robust to the perturbation of the first measurement and can be read out precisely [Fig. 1(a)]. Here we utilize the charge state as this robust state and exploit the spin-to-charge conversion (SCC) technique [35–37]. We demonstrate the first-ever implementation of a single-shot readout of spin qutrit by performing fast spin-selective ionization followed by a single-shot readout of both the spin and charge states. Using this technique, we demonstrate a genuine single-particle verification of the quantum contextuality based on the solid-state electron spin qutrit.

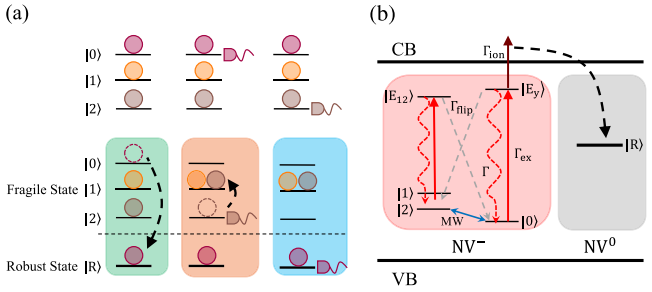

FIG. 1. Schematic diagram for qutrit readout. (a) Schematic diagram of binary qutrit readout scheme with nondemolition measurement (top) and with a robust state conversion shown in the green box (bottom). The original population of qutrit states are denoted by balls with different colors ($|0\rangle$: purple, $|1\rangle$: orange, $|2\rangle$: brown). The qutrit state can be read out via two nondemolition measurements (top medium and top right) without disturbing the original state or a combination of spin state readout (bottom medium) and charge state readout (top right) after a state conversion (bottom left). The dashed circumference denotes the population which is transferred to other states. (b) Energy level structure of the NV center. The NV^- (NV^0) structure is shown in the red (gray) box. The internal structure of NV^0 is omitted. The conduction and valence band are denoted as CB and VB, respectively. The excitation (red arrow) and fluorescence (wavy arrow) of $|0\rangle$ and $\{|1\rangle, |2\rangle\}$ are labeled as E_y and E_{12}, respectively. The spin-flip process is denoted by the gray arrow. The dark red and black arrows represent ionization and the subsequent process of returning to NV^0. The unitary operation between $|0\rangle$ and $|1\rangle(|2\rangle)$ is achieved by resonant microwave pulse (blue arrow).

Critically, we observe a violation of the classical boundary with our single-shot readout, but no violation with the conventional readout. The readout technique thus provides an important tool for developing qutrit information processing.

Our approach consists of three independent processes, a high fidelity SCC, a spin state readout, and a high fidelity charge state readout [Figs. 1(a) and 1(b)]. The essence of SCC is a spin-selective two-photon ionization process. Among qutrit states $\{|0\rangle, |1\rangle, |2\rangle\}$ (corresponding to the ground states $\{|m_s = 0\rangle, |m_s = +1\rangle, |m_s = -1\rangle\}$), the state $|0\rangle$ is selectively and resonantly excited to $|E_y\rangle$ via an E_y laser pulse and simultaneously ionized to NV^0 using another intense ionization pulse. After the conversion, the qutrit states NV^-: $\{|1\rangle, |2\rangle\}$ and NV^0: $|0\rangle$ are then subsequently determined via two binary measurements of the spin state and charge state, respectively.

Although demonstrated, the fidelity of SCC is limited to 78% due to the low ionization rate [35]. Here we first achieve a high-fidelity SCC with a high-power 642 nm ionization laser while suppressing the laser-induced spectral drift. The experimental procedure consists of environment stabilization, spectrum tracking, and individual experiment [Fig. 2(a)]. During the environment stabilization, a 45 mW, 642 nm laser is continuously applied in a range of several microns around the NV center for 60 min, leading to a long-lived (> 12 h) stable environment and spectrum. Without the environment stabilization process, we observe a random spectral diffusion due to 642 nm laser illumination [Fig. 2(d)]. Importantly, this spectral diffusion is an instantaneous effect rather than a slow drift as verified by applying a high-power 10 μs 642 nm laser pulse between two consecutive charge state readouts [Fig. 2(b)]. The distribution of two readouts shows no correlation [Fig. 2(f)], indicating that the tracked spectrum drifts after applying the 10 μs 642 nm laser pulse, which leads to the incorrect second charge state readout and misinterpretation of $|1\rangle$ SCC result [Fig. 2(h)]. In contrast, the spectrum becomes stable with the environment stabilization process [Fig. 2(e)]. The charge state shows the expected correlation [Fig. 2(g)] and the charge state readout fidelity achieves $99.63 \pm 0.07\%$. We attribute the spectral diffusion to the dynamics of local electronic defects' charge state. The long-time 642 nm illumination drives such a local charge environment into a steady state. Our technique thus benefits in applications involving resonant optical excitation in quantum sensing or quantum network.

With the reliable charge state readout, we then characterize the high-fidelity SCC process using the sequence in Fig. 2(c). As expected, $|0\rangle$ is ionized within tens of microseconds, while $|1\rangle$ and $|2\rangle$ remain mostly (> 96%) in the NV^- state [Fig. 2(i)]. The slight ionization of $|1\rangle$ ($|2\rangle$) results from the off-resonance excitation of E_y laser. The SCC fidelity of state $|0\rangle$ reaches $92.87 \pm 0.34\%$. The extracted ionization rate Γ_{ion} (see Supplemental Material [38] Sec. VI) is still linearly dependent on the laser power [Fig. 2(i)], indicating that 642 nm laser alone cannot ionize the spin state via a double photon process. This property allows the fidelity to be further improved by increasing laser power. The linear coefficient of 218.2 ± 15.8 kHz/mW for 642 nm laser is much higher than the coefficient of 67.0 ± 6.7 kHz/mW for NIR laser [35], which confirms theoretical predictions [43].

We next demonstrate a high-fidelity qutrit readout using the sequence in Fig. 3(a), which includes initialization of both charge state and spin state, SCC, repetitive spin state readout, and charge state readout. After 10 μs SCC, the $|0\rangle$ state is ionized to NV^0 while the $|1\rangle$ and $|2\rangle$ states remain in NV^-. During the spin readout process, the state $|2\rangle$ is flipped to $|0\rangle$ via a microwave π pulse and then readout by an E_y pulse, whereas the $|1\rangle$ state still remains dark. To suppress the spin-flip error, the leakage population from $|0\rangle$ to $|2\rangle$ is transferred back to $|0\rangle$ by another π pulse for the subsequent readout. The results of this spin readout scheme are shown in Fig. 3(c), where the maximum average fidelity is achieved with two repeats. In combination with the charge state readout, the qutrit state is then determined in a single-shot readout from four outcomes [Fig. 3(d)]. We note that the fourth unspecified item is helpful in joint probability measurements and will be elaborated later.

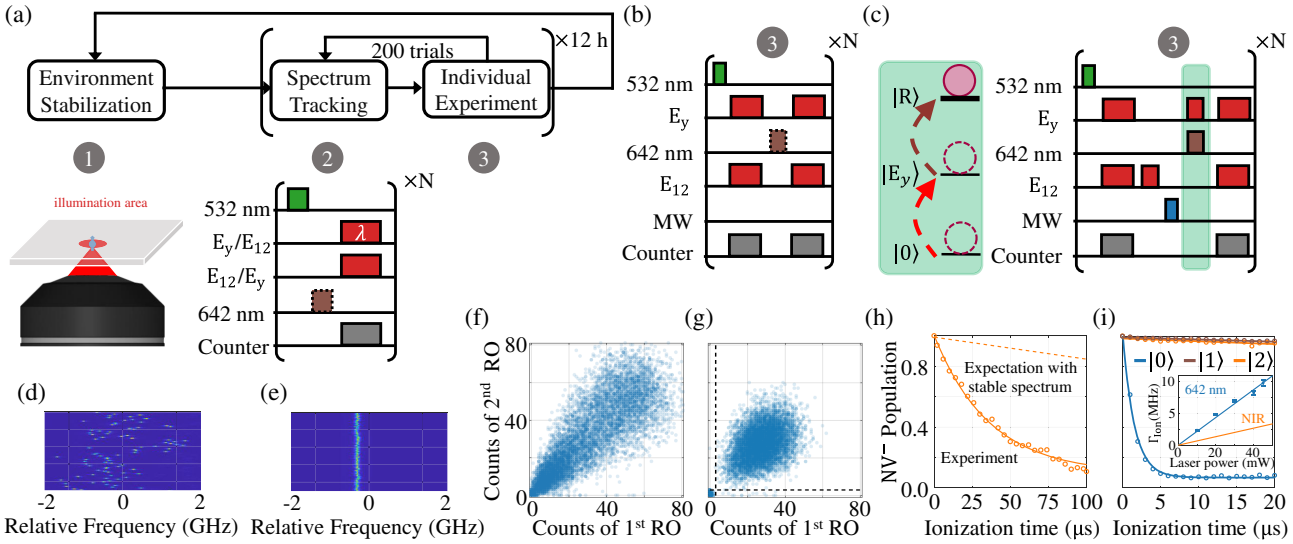

FIG. 2. High-fidelity SCC using the high-power ionization laser. (a) Schematic diagram of the experimental framework including environment stabilization, spectrum tracking, and individual experiments. The spectrums of E_y and E_{12} are updated every 200 trials of individual experiments. A 10 μs pulse of 642 nm laser (45 mW) is applied in spectrum tracking to maintain the stabilized environment. (b) Pulse sequence for consecutive charge state readout. A 2 μs pulse of 532 nm laser is applied to reset the charge state of NV center. A 200 μs E_y and E_{12} pulses generate fluorescence when NV center stays in the NV^- state, which is detected by the counter. A 10 μs pulse of 642 nm laser (45 mW) is applied to verify the spectral stability. (c) Pulse sequence for the ionization efficiency characterization. After a measurement-based charge state initialization, the spin state is initialized on demand using a E_{12} and a microwave π pulse. The SCC (green box) is achieved by a multicolor laser pulse of E_y and 642 nm laser, which is verified by a second charge state readout. (d)–(e) Photoluminescence spectrum without and with environment stabilization. A pulse consisting of 10 μs 642 nm (45 mW) laser and 1 ms idling is applied 2000 times in the interval between two adjacent scans. (f)–(g) The correlation between the two consecutive charge readouts without and with environment stabilization. The experimental sequence is shown in (b). Each datum corresponds to the quantity of collected photons in two consecutive readouts emanating from a singular experimental trial. The NV^0 and NV^- state, corresponding to the dark and bright states, are indistinguishable without environment stabilization, and highly distinguishable with an average fidelity of $99.63 \pm 0.07\%$ using the threshold marked by the dashed black lines with environment stabilization. (h) Ionization curve of $|1\rangle$ without environment stabilization. The dashed line represents the expectation with a stable spectrum, which differs greatly from the experimental results (orange circle) due to the limited fidelity charge state readout in (f). The solid line is an exponential fit to experimental results. (i) Ionization curves with environment stabilization. The solid line for $|0\rangle$ is a simulation using a seven-dimensional model. The solid lines for $|1\rangle$ and $|2\rangle$ are linear fits. Inset: The dependence of the ionization rate Γ_{ion} on laser power. The blue line is a linear fit with a coefficient of 218.2 ± 15.8 kHz/mW. The yellow line represents Γ_{ion} in [35].

The average readout fidelity of qutrit is $87.80 \pm 0.36\%$ [Figs. 3(e)–3(g)]. To quantify the readout imperfections, we summarize the fidelities of these independent processes in Fig. 3(h). The expectation coincides well with experimental results (see Supplemental Material [38] Sec. VII). The average fidelity is mainly limited by the spin-flip process. This process occasionally transforms the spin state, leading to a decrease in the fidelity of both the SCC and spin state readout processes. The dependence of final readout fidelity on the spin-flip rate is shown in Fig. 3(b). The small deviation between simulation and experiment originates from high background counts and off-resonance excitation of the E_y laser. The average fidelity can be improved to 97.34% with a low spin-flip rate NV center [23].

We use the single-shot readout to investigate contextuality. Contextuality reflects the divergence between quantum mechanics and the noncontextual hidden variable (NCHV) model in an indivisible system. The NCHV model assumes that measurement outcomes are determined by hidden variables, and is conflicting with the prediction of quantum mechanics. Although Kochen and Specker first proposed a contextuality test [44], experimental verification was ambiguous until the discovery of noncontextuality inequalities [45]. Different from other systems such as the photonic system [12,13,46], superconducting system [15], NMR system [47] and trapped ions [14], the contextuality test in the NV center is lacking due to the issue in joint probability measurement. With our qutrit single-shot readout scheme, we perform a fundamental test of contextuality based on the electron spin qutrit of NV center in diamond.

The verification scheme is achieved by measuring five properly chosen observables [45]. The theoretical framework is equivalent to proving that the following inequality holds (see Supplemental Material [38] Sec. VIII):

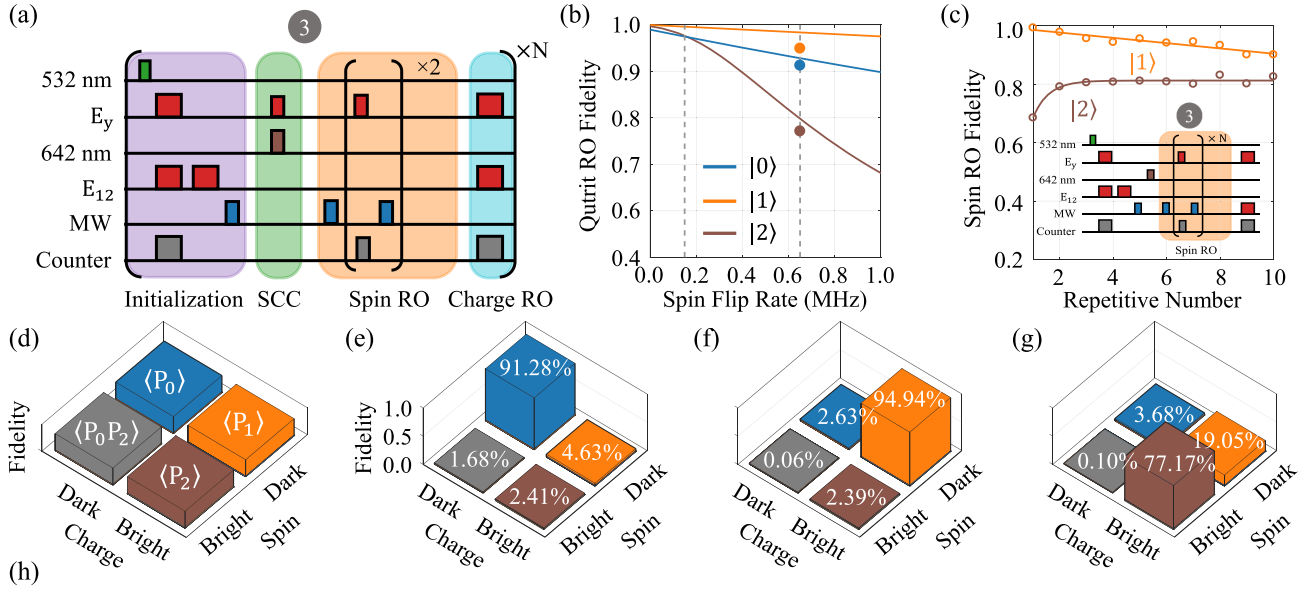

(h)

Qutrit state	SCC	Spin RO	Charge RO	Expectation	Qutrit RO
$\|0\rangle$	92.87±0.34%	97.57±0.18%	99.42±0.14%	90.33±1.55%	91.28±0.34%
$\|1\rangle$	97.73±0.46%	97.57±0.18%	99.82±0.04%	95.44±1.83%	94.94±0.22%
$\|2\rangle$	96.57±0.66%	78.95±0.84%	99.82±0.04%	76.11±1.40%	77.17±0.53%

FIG. 3. Single-shot readout of qutrit state. (a) Pulse sequence for qutrit readout, including initialization of charge state and spin state, SCC, spin state readout (Spin RO) and charge state readout (Charge RO). (b) Dependence of qutrit readout fidelity on the spin-flip rate. The measured readout fidelities are marked with dots. The dashed gray lines mark the expected fidelity corresponding to a spin-flip rate of 0.66 MHz observed in this work and a low spin-flip rate of 0.15 MHz reported in [23], respectively. (c) Spin state readout fidelity dependence on the repetitive number. The $|1\rangle$ and $|2\rangle$ states are denoted as dark and bright state, respectively. Inset: sequence for repetitive spin state readout. (d) Correspondence between qutrit states and results of two binary readouts. P_i is the projective operator $|i\rangle\langle i|$ $(i = 0, 1, 2)$. (e)–(g) Readout fidelity of $|0\rangle$, $|1\rangle$, and $|2\rangle$. (h) Fidelity of qutrit readout process.

$$\sum_{i=1}^{5}\langle L_i\rangle_{\psi_0} - \sum_{i=1}^{5}\langle L_i L_{i+1}\rangle_{\psi_0} > 2. \tag{1}$$

The five observables L_i are projective operators and given by $L_i = \mathbb{1} - S_{l_i}^2 = |\boldsymbol{l}_i\rangle\langle\boldsymbol{l}_i|$ with $L_6 = L_1$, where $\boldsymbol{l}_i$ denotes a cyclic quintuplet of unit vectors with $\boldsymbol{l}_i \perp \boldsymbol{l}_{i+1}$ $(i = 1, \ldots, 5)$. $|\psi_0\rangle$ is a certain neutrally polarized state. A schematic of ψ_0 and $\boldsymbol{l}_i$ is shown in Fig. 4(a). The expectations are evaluated with $\langle L_i\rangle_{\psi_0} = \langle\psi_0|L_i|\psi_0\rangle$ and $\langle L_i L_{i+1}\rangle_{\psi_0} = \langle\psi_0|\boldsymbol{l}_i\rangle\langle\boldsymbol{l}_i|\boldsymbol{l}_{i+1}\rangle\langle\boldsymbol{l}_{i+1}|\psi_0\rangle$. The joint probability measurement $\langle L_i L_{i+1}\rangle_{\psi_0}$ usually requires two consecutive readouts in which the first measurement needs to be nondemolition. In our readout scheme, this joint probability is mapped to the population and measured in one experimental trial.

A proper choice of L_i shows $\langle L_i\rangle_{\psi_0} = 1/\sqrt{5}$, and the sum of left terms in inequality (1) should be $\sqrt{5}$ theoretically. However, the state $|\boldsymbol{l}_i\rangle$ could be nonorthogonal with $|\boldsymbol{l}_{i+1}\rangle$ due to the imperfections during the experiment, and the observable L_6 may also differ from L_1. Therefore $\langle L_i L_{i+1}\rangle_{\psi_0}$ cannot be omitted and the inequality (1) turns into (see Supplemental Material [38] Sec. VIII)

$$\sum_{i=1}^{5}\langle L_i\rangle_{\psi_0} - \sum_{i=1}^{5}\langle L_i L_{i+1}\rangle_{\psi_0} + \langle L_6 L_1\rangle_{\psi_0} - 0.5(\langle L_1\rangle_{\psi_0} + \langle L_6\rangle_{\psi_0}) = \sqrt{5} > 2. \tag{2}$$

The states $|\boldsymbol{l}_i\rangle$ are given as $|\boldsymbol{l}_1\rangle = |1\rangle$, $|\boldsymbol{l}_2\rangle = |2\rangle$, $|\boldsymbol{l}_3\rangle = R_a(-\gamma)|\boldsymbol{l}_1\rangle$, $|\boldsymbol{l}_4\rangle = R_a(-\gamma)R_b(-\gamma)|\boldsymbol{l}_2\rangle$, $|\boldsymbol{l}_5\rangle = R_a(-\gamma)R_b(-\gamma)|\boldsymbol{l}_3\rangle$, $|\boldsymbol{l}_6\rangle = R_a(-\gamma)R_b(-\gamma)|\boldsymbol{l}_4\rangle = |\boldsymbol{l}_1\rangle$, where $\gamma = \arccos(2 - \sqrt{5})$ and $R_a(\theta)$ $[R_b(\theta)]$ represents a unitary rotation operation around the X axis in $\{|0\rangle, |1\rangle\}$ $(\{|0\rangle, |2\rangle\})$. The experimental sequence is shown in Fig. 4(b). The neutrally polarized state $|\psi_0\rangle$ is first prepared from $|0\rangle$ using $U = R_a(\phi)R_b(-\theta)$ with $\theta = \arccos[1 - (2/\sqrt{5})]$ and $\phi = \arccos[(1 - \sqrt{5})/2]$. Next, a unitary operations U_i (Table I) will map qutrit basis $\{|0\rangle, |1\rangle, |2\rangle\}$ into $\{|\boldsymbol{l}_i\rangle, |\boldsymbol{l}_i \times \boldsymbol{l}_{i+1}\rangle, |\boldsymbol{l}_{i+1}\rangle\}$ [Fig. 4(c)]. $\langle L_i\rangle_{\psi_0}$ and $\langle L_{i+1}\rangle_{\psi_0}$ are then obtained by measuring the population of the state $|0\rangle$ and $|2\rangle$, while $\langle L_i L_{i+1}\rangle$ is directly obtained

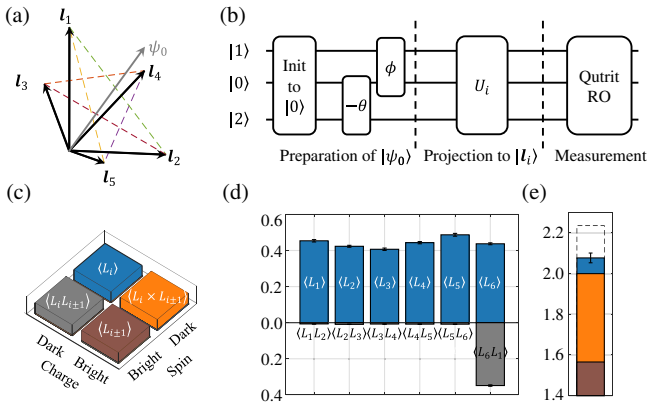

FIG. 4. Contextuality verification with the single electron spin qutrit. (a) Regular pentagram of cyclic quintuplet of unit vectors. Each dashed line corresponds to a right angle formed by $\boldsymbol{l}_i$ and $\boldsymbol{l}_{i+1}$. ψ_0 coincides with the symmetry axis of the pentagram. (b) Pulse sequences for the test of the NCHV model. (c) Correspondence between observable and results of single shot readout. (d) Experimental results of observable in inequality (2). (e) The sum of the left term of inequality (2). The blue bar corresponds to violations indicated by experimental results in (d). The orange bar shows the prediction of NCHV model. The brown bar shows the expected value using two conventional consecutive measurements. The dashed bar represents the result of a perfect experiment.

by measuring the fourth outcome in our single-shot readout, avoiding the loophole in the conventional readout scheme (see Supplemental Material [38] Sec. IX).

The experimental results are shown in Fig. 4(d), and inequality (2) turns into

$$\sum_{i=1}^{5}\langle L_i\rangle_{\psi_0}-\sum_{i=1}^{5}\langle L_iL_{i+1}\rangle_{\psi_0}+\langle L_6L_1\rangle_{\psi_0}-0.5(\langle L_1\rangle_{\psi_0}+\langle L_6\rangle_{\psi_0})=2.077\pm0.024>2. \quad (3)$$

This final result shows the violation of the NCHV inequality by about 3.2 times of the standard deviation. However, the verification with conventional readout averages all results (see Supplemental Material [38] Sec. XI). Thus the conventional readout would only reach 1.565 even assuming a perfect experiment, indicating no violation of the NCHV model.

TABLE I. Unitary operation involved in contextuality verification.

i	U_i
1	$R_a(\pi)$
2	$R_a(\gamma)R_b(\pi)$
3	$R_b(\gamma)R_a(\gamma)R_a(\pi)$
4	$R_a(\gamma)R_b(\gamma)R_a(\gamma)R_b(\pi)$
5	$R_b(\gamma)R_a(\gamma)R_b(\gamma)R_a(\gamma)R_a(\pi)$

In summary, we successfully demonstrate a binary readout scheme for the single-shot readout of the high-dimensional quantum system using robust ancillary states without the nondemolition measurement requirement. As a general readout scheme, our scheme can be extended to other degrees of freedom like nuclear spin states, as long as this degree of freedom can be measured independently. Besides quantum contextuality, our results benefit a broad range of high-spin-based applications, such as simulating topological Euler insulators [48] and observing the tensor monopoles [49]. Our approach could also enable the realization of a qutrit-based quantum algorithm [50]. Apart from quantum information processing, our results also contribute to investigating the essence and dynamical behavior of high-dimensional quantum correlations [51,52].

This work is supported by the National Natural Science Foundation of China (Grants No. T2325023, No. 92265204, No. T2125011, No. 12104446, No. 12104447, No. 12261160569), the CAS (GJJSTD20200001), the Innovation Program for Quantum Science and Technology (Grant No. 2021ZD0302200), the Anhui Initiative in Quantum Information Technologies (Grant No. AHY050000), the Fundamental Research Funds for the Central Universities.

J. D. and Y. W. supervised the project and the experiment; Y. W. and X. K. conceived the ideas; Y. G. and W. J. built the setup; M. W. and H. S. prepared the sample; Y. G. and J. Z. performed the experiments; Y. G. and Z. C. conducted the simulations; Y. W., Y. G., and W. J. wrote the manuscript. All authors analyzed the data and revised the manuscript.

*kongxi@nju.edu.cn
†ywustc@ustc.edu.cn
‡djf@ustc.edu.cn

[1] V. D'ambrosio, E. Nagali, S. P. Walborn, L. Aolita, S. Slussarenko, L. Marrucci, and F. Sciarrino, Nat. Commun. **3**, 961 (2012).
[2] T. M. Graham, H. J. Bernstein, T.-C. Wei, M. Junge, and P. G. Kwiat, Nat. Commun. **6**, 7185 (2015).
[3] Y.-H. Luo, H.-S. Zhong, M. Erhard, X.-L. Wang, L.-C. Peng, M. Krenn, X. Jiang, L. Li, N.-L. Liu, C.-Y. Lu, A. Zeilinger, and J.-W. Pan, Phys. Rev. Lett. **123**, 070505 (2019).
[4] X.-M. Hu, C. Zhang, B.-H. Liu, Y. Cai, X.-J. Ye, Y. Guo, W.-B. Xing, C.-X. Huang, Y.-F. Huang, C.-F. Li, and G.-C. Guo, Phys. Rev. Lett. **125**, 230501 (2020).
[5] E. T. Campbell, Phys. Rev. Lett. **113**, 230501 (2014).
[6] H. Bechmann-Pasquinucci and A. Peres, Phys. Rev. Lett. **85**, 3313 (2000).
[7] A. Fedorov, L. Steffen, M. Baur, M. P. da Silva, and A. Wallraff, Nature (London) **481**, 170 (2012).
[8] B. P. Lanyon, M. Barbieri, M. P. Almeida, T. Jennewein, T. C. Ralph, K. J. Resch, G. J. Pryde, J. L. O'brien, A. Gilchrist, and A. G. White, Nat. Phys. **5**, 134 (2009).

[9] S. Rosenblum, P. Reinhold, M. Mirrahimi, L. Jiang, L. Frunzio, and R. J. Schoelkopf, Science **361**, 266 (2018).

[10] N. J. Cerf, S. Massar, and S. Pironio, Phys. Rev. Lett. **89**, 080402 (2002).

[11] A. C. Dada, J. Leach, G. S. Buller, M. J. Padgett, and E. Andersson, Nat. Phys. **7**, 677 (2011).

[12] R. Lapkiewicz, P. Li, C. Schaeff, N. K. Langford, S. Ramelow, M. Wieśniak, and A. Zeilinger, Nature (London) **474**, 490 (2011).

[13] X.-X. Chen, J. Li, M. Aili, Z. Meng, Y.-J. Wang, and A.-N. Zhang, Phys. Rev. A **107**, 042431 (2023).

[14] P. Wang, J. Zhang, C.-Y. Luan, M. Um, Y. Wang, M. Qiao, T. Xie, J.-N. Zhang, A. Cabello, and K. Kim, Sci. Adv. **8**, eabk1660 (2022).

[15] M. Jerger, Y. Reshitnyk, M. Oppliger, A. Potočnik, M. Mondal, A. Wallraff, K. Goodenough, S. Wehner, K. Juliusson, N. K. Langford *et al.*, Nat. Commun. **7**, 12930 (2016).

[16] M. S. Blok, V. V. Ramasesh, T. Schuster, K. O'Brien, J. M. Kreikebaum, D. Dahlen, A. Morvan, B. Yoshida, N. Y. Yao, and I. Siddiqi, Phys. Rev. X **11**, 021010 (2021).

[17] A. R. Shlyakhov, V. V. Zemlyanov, M. V. Suslov, A. V. Lebedev, G. S. Paraoanu, G. B. Lesovik, and G. Blatter, Phys. Rev. A **97**, 022115 (2018).

[18] M. Ringbauer, M. Meth, L. Postler, R. Stricker, R. Blatt, P. Schindler, and T. Monz, Nat. Phys. **18**, 1053 (2022).

[19] J. R. Maze, P. L. Stanwix, J. S. Hodges, S. Hong, J. M. Taylor, P. Cappellaro, L. Jiang, M. G. Dutt, E. Togan, A. Zibrov *et al.*, Nature (London) **455**, 644 (2008).

[20] I. Lovchinsky, A. Sushkov, E. Urbach, N. P. de Leon, S. Choi, K. De Greve, R. Evans, R. Gertner, E. Bersin, C. Müller *et al.*, Science **351**, 836 (2016).

[21] T. Staudacher, F. Shi, S. Pezzagna, J. Meijer, J. Du, C. A. Meriles, F. Reinhard, and J. Wrachtrup, Science **339**, 561 (2013).

[22] F. Shi, Q. Zhang, P. Wang, H. Sun, J. Wang, X. Rong, M. Chen, C. Ju, F. Reinhard, H. Chen *et al.*, Science **347**, 1135 (2015).

[23] P. C. Humphreys, N. Kalb, J. P. Morits, R. N. Schouten, R. F. Vermeulen, D. J. Twitchen, M. Markham, and R. Hanson, Nature (London) **558**, 268 (2018).

[24] S. Hermans, M. Pompili, H. Beukers, S. Baier, J. Borregaard, and R. Hanson, Nature (London) **605**, 663 (2022).

[25] H. Bernien, B. Hensen, W. Pfaff, G. Koolstra, M. S. Blok, L. Robledo, T. H. Taminiau, M. Markham, D. J. Twitchen, L. Childress *et al.*, Nature (London) **497**, 86 (2013).

[26] A. Tchebotareva, S. L. N. Hermans, P. C. Humphreys, D. Voigt, P. J. Harmsma, L. K. Cheng, A. L. Verlaan, N. Dijkhuizen, W. de Jong, A. Dréau, and R. Hanson, Phys. Rev. Lett. **123**, 063601 (2019).

[27] C. Bradley, S. de Bone, P. Möller, S. Baier, M. Degen, S. Loenen, H. Bartling, M. Markham, D. Twitchen, R. Hanson *et al.*, npj Quantum Inf. **8**, 122 (2022).

[28] C. E. Bradley, J. Randall, M. H. Abobeih, R. C. Berrevoets, M. J. Degen, M. A. Bakker, M. Markham, D. J. Twitchen, and T. H. Taminiau, Phys. Rev. X **9**, 031045 (2019).

[29] B. Hensen, H. Bernien, A. E. Dréau, A. Reiserer, N. Kalb, M. S. Blok, J. Ruitenberg, R. F. Vermeulen, R. N. Schouten, C. Abellán *et al.*, Nature (London) **526**, 682 (2015).

[30] B. Hensen, N. Kalb, M. Blok, A. Dréau, A. Reiserer, R. Vermeulen, R. Schouten, M. Markham, D. Twitchen, K. Goodenough *et al.*, Sci. Rep. **6**, 30289 (2016).

[31] S. B. van Dam, J. Cramer, T. H. Taminiau, and R. Hanson, Phys. Rev. Lett. **123**, 050401 (2019).

[32] Y. Fu, W. Liu, X. Ye, Y. Wang, C. Zhang, C.-K. Duan, X. Rong, and J. Du, Phys. Rev. Lett. **129**, 100501 (2022).

[33] S. Hernández-Gómez, S. Gherardini, N. Staudenmaier, F. Poggiali, M. Campisi, A. Trombettoni, F. Cataliotti, P. Cappellaro, and N. Fabbri, PRX Quantum **3**, 020329 (2022).

[34] L. Robledo, L. Childress, H. Bernien, B. Hensen, P. F. Alkemade, and R. Hanson, Nature (London) **477**, 574 (2011).

[35] Q. Zhang, Y. Guo, W. Ji, M. Wang, J. Yin, F. Kong, Y. Lin, C. Yin, F. Shi, Y. Wang *et al.*, Nat. Commun. **12**, 1529 (2021).

[36] D. M. Irber, F. Poggiali, F. Kong, M. Kieschnick, T. Lühmann, D. Kwiatkowski, J. Meijer, J. Du, F. Shi, and F. Reinhard, Nat. Commun. **12**, 532 (2021).

[37] C. P. Anderson, E. O. Glen, C. Zeledon, A. Bourassa, Y. Jin, Y. Zhu, C. Vorwerk, A. L. Crook, H. Abe, J. Ul-Hassan *et al.*, Sci. Adv. **8**, eabm5912 (2022).

[38] See Supplemental Material at http://link.aps.org/supplemental/10.1103/PhysRevLett.132.060601, for details in the environment stabilization, the derivation of the NCHV inequality and the experimental setup, which includes Refs. [39–42].

[39] I. Meirzada, Y. Hovav, S. A. Wolf, and N. Bar-Gill, Phys. Rev. B **98**, 245411 (2018).

[40] N. Kalb, P. C. Humphreys, J. J. Slim, and R. Hanson, Phys. Rev. A **97**, 062330 (2018).

[41] L. Robledo, H. Bernien, T. Van Der Sar, and R. Hanson, New J. Phys. **13**, 025013 (2011).

[42] P. Neumann, J. Beck, M. Steiner, F. Rempp, H. Fedder, P. R. Hemmer, J. Wrachtrup, and F. Jelezko, Science **329**, 542 (2010).

[43] L. Razinkovas, M. Maciaszek, F. Reinhard, M. W. Doherty, and A. Alkauskas, Phys. Rev. B **104**, 235301 (2021).

[44] S. Kochen and E. P. Specker, J. Math. Mech. **17**, 59 (1967), http://www.jstor.org/stable/24902153.

[45] A. A. Klyachko, M. A. Can, S. Binicioğlu, and A. S. Shumovsky, Phys. Rev. Lett. **101**, 020403 (2008).

[46] B. H. Liu, Y. F. Huang, Y. X. Gong, F. W. Sun, Y. S. Zhang, C. F. Li, and G. C. Guo, Phys. Rev. A **80**, 044101 (2009).

[47] S. Dogra, K. Dorai *et al.*, Phys. Lett. A **380**, 1941 (2016).

[48] W. Zhao, Y.-B. Yang, Y. Jiang, Z. Mao, W. Guo, L. Qiu, G. Wang, L. Yao, L. He, Z. Zhou *et al.*, Commun. Phys. **5**, 223 (2022).

[49] X. Tan, D.-W. Zhang, W. Zheng, X. Yang, S. Song, Z. Han, Y. Dong, Z. Wang, D. Lan, H. Yan, S.-L. Zhu, and Y. Yu, Phys. Rev. Lett. **126**, 017702 (2021).

[50] T. Roy, Z. Li, E. Kapit, and D. I. Schuster, arXiv:2211.06523.

[51] G. De Chiara and A. Sanpera, Rep. Prog. Phys. **81**, 074002 (2018).

[52] R. Auccaise, L. C. Céleri, D. O. Soares-Pinto, E. R. deAzevedo, J. Maziero, A. M. Souza, T. J. Bonagamba, R. S. Sarthour, I. S. Oliveira, and R. M. Serra, Phys. Rev. Lett. **107**, 140403 (2011).